DOI: 10.17344/acsi.2022.7517 *Acta Chim. Slov.* **2022,** *69,* 638–646

Scientific paper

Electroanalytical Determination of Ziram by Differential Pulse Voltammetry with Reduced Graphene Oxide/Gold Nanoparticles Modified Glassy Carbon Electrode

Nazife Aslan,[1]* Sema Bilge Ocak[2] and Uğur Gökmen[3]

[1] *Ankara Hacı Bayram Veli University, Polatlı Science and Arts Faculty, Department of Chemistry, 06900 Ankara, Turkey*

[2] *Gazi University, Graduate School of Natural and Applied Sciences, 06560 Ankara, Turkey*

[3] *Gazi University, Faculty of Technology Metallurgical and Materials Engineering, 06500 Ankara, Turkey*

* *Corresponding author: E-mail: nazife.aslan@hbv.edu.tr*

Received: 04-04-2022

Abstract

The preparation of gold nanoparticles-reduced graphene oxide-based sensor materials for the determination of zinc(II) dimethyldithiocarbamate (ziram) is described in this paper. The graphene oxide (GO) was synthesized using a modified Hummer's method. A composite sensor consisting of gold nanoparticles (AuNPs) and reduced graphene oxide (RGO) was electrochemically fabricated on a glassy carbon electrode. The nanocomposite was evaluated utilizing scanning electron microscopy (SEM). Cyclic voltammetry was used to illuminate the modified sensor's electrochemical properties at each stage of the modification. The suggested sensor was demonstrated good analytical performance to determine ziram pesticide in water and peach juice, including a very low detection limit, a large linear range, and a low RSD.

Keywords: Reduced graphene oxide; ziram; nanomaterials; sensors

1. Introduction

Materials having sizes or properties ranging from 1 to 100 nm in one or more dimensions are called nanomaterials. Superior thermal, mechanical, electrical, and biological properties not available in conventional materials are the important characteristics of these materials.[1]

The combination of these distinctive properties with their remarkable recognition abilities has resulted in improved performance. Apart from their high mechanical strength and low weight, nanomaterials' surface features, including area, roughness, energetics, and electron distributions, are primarily the result of their unique properties. It is obvious that nanomaterials, which has applications such as providing clean drinking water, improving air quality, developing new energy sources and at the same time removing dangerous and toxic substances from our environment, will help create a sustainable environment.[2]

Graphene is one of the most important nanomaterials, with a wide range of applications that are expanding.[3,4] It is made up of sp^2 bonded carbon atoms with a single atom thickness, as is well known. As a result of these characteristics, it exhibits remarkable electron transport capability and catalytic behavior for particular chemicals. Overall, due to its high spesific surface area, low cost, ease of processing and safety, and superior electrical conductivity, it can play a vital role in increasing the performance of sensors.[5,6] With its potential application areas, it is one of the most investigated materials nowadays.[7] Graphene, on the other hand, is hydrophobic and does not form stable dispersions in polar solvents.[8] This severely limits its use in sensor development. An effective method for overcoming this problem is in situ chemical or electrochemical reduction of highly hydrophilic graphene oxide (GO) to produce graphene.[9] The electrochemical reduction method is commonly used because it is a green process that does not require a strong chemical reducing agent.[10]

Metal nanoparticles (NP) have qualities that are determined by their size and form. Chemical and biosensors, catalyst synthesis, electronic device component preparation, imaging systems, medical and environmental applications all use a variety of metal NPs in various sizes, forms, and morphologies.[11,12] Among them gold nanoparticles (AuNPs) have been received great interests as sensor

devices due to its high selectivity, sensitivity, biocompability and excellent chemical stability. Especially, the introduction of AuNPs into modified electrodes has obvious advantages in improving the sensor performances.[13,14] It has been stated in the literature that sensors made with reduced graphen oxide (RGO)-metal nanocomposites superior qualities such as sensitivity, lower detection limits, and faster electron transfer kinetics.[15,16] RGO has hydroxyl (-OH) and carboxylate (-COOH) groups in its structure, which allows it to interact with metal nanoparticles to create a metal nanoparticle-graphene based electrochemical sensor.[17,18] Therefore, AuNPs/RGO have recently been used in electrochemical sensors for pesticide and other organic and inorganic pollutant detection.[19–24]

Pesticides are widely employed as agrochemicals to enhance agricultural production by controlling or killing insects, pests, and fungi. Uncontrolled pesticide use, on the other hand, could endanger public health.[25,26] Ziram is a dithiocarbamate (DTC) fungicide that is commonly used to control moulds, black spot, rot, and blight, as well as to maintain the quality of fruits and vegetables throughout transit and storage. Ziram residues, on the other hand, can cause major health problems, such as headaches and nausea, as well as cancer. It's also linked to skin allergies, asthma, Parkinson's disease risk, and inflammation of the eyes and respiratory tract.[27–32]

Several analytical instruments, such as high-performance liquid chromatography followed by atomic absorption spectrometry (HPLC-AAS),[33] liquid chromatography-mass spectrometry (LC-MS/MS),[34] and gas chromatography–mass spectrometry (GC–MS),[35] gas chromatography-electron capture detector (GC-ECD),[36] inductively coupled plasma mass spectrometry[37] are widely used in monitoring environmental contaminants such as ziram in agricultural products. Electrochemical detection[38–43] and immunoassays[44] are some of the other rapid methods for detecting trace compounds that have been proposed. Because of their numerous advantages, such as rapid response, a wide dynamic range, portability, ease of modification, and low cost, electrochemical sensors are a viable and rapid instrument for detecting pesticide residues in food and environmental samples.

The goal of this research was to explore if composites of reduced graphene oxide and gold nanoparticles might be employed as an electrochemical sensor material for low-concentration voltammetry-based pesticide residue monitoring. A glassy carbon electrode (GCE) modified with RGO and AuNPs was used to create and measure a new voltammetric sensor for the determination of ziram. The results indicated that the AuNPs/RGO-modified glassy carbon electrode could provide a quick and easy platform for ziram detection with high sensitivity, fast response, and wide detection range. So far, only a few electrochemical methods for the detection of ziram using nanocomposite sensors have been published, and real sample applications in foods are extremely limited.[45,46] As a result, it is critical to develop new methods that will serve as an alternative to existing analysis methods.

Using a scanning electron microscope, the surface specimens of the produced RGO/AuNPs/GCE were examined. For AuNPs electrodeposition and ziram determination, cyclic voltammetry (CV) and differential pulse voltammetry (DPV) were utilized. Furthermore, limit of detection, limit of quantification, linearity, repeatability, reproducibility and pH of the sensor were investigated in detail. The RGO/AuNPs/GCE has been successfully used as electrochemical sensor to determining of ziram fungicide in peach juice and tap water samples.

2. Experimental

2. 1. Reagents

Graphite (Alfa Aeser, <20 μm), $HAuCl_4.H_2O$ 99.995%, zinc(II) dimethylditiyocarbamate (99.9%), $K_3[Fe(CN)_6]$, $K_4[Fe(CN)_6]$, hydrogen peroxide, boric acid, o-phosphoric acid and sulfuric acid were provided by Sigma Aldrich; Merck supplied sodium nitrate ($NaNO_3$), potassium permanganate ($KMnO_4$), sodium hydroxide, sodium acetate, hydrochloric acid, sodium dihydrogenphosphate.$2H_2O$, sodium monohydrogenphosphate.$7H_2O$ and potassium chloride. The Britton Robinson (BR) buffer solution and all other solutions were made with ultrapure water. All experiments were carried out at room temperature. All sensor applications were performed in BR buffer with a pH of 8.0 and 100 mM KCl as a supporting electrolyte.

2. 2.Instrumentation

The CH Instruments 660B model Ivium potentiostat/galvanostat Electrochemical Analyzer (Ivium Technologies, Netherlands) was used for all electrochemical experiments. A triple electrode system was used in the experiments, including an Ag/AgCl reference electrode, a glassy carbon working electrode, and a Pt wire counter electrode.

Carl Zeiss AG's EVO® 50 Series was used to capture scanning electron microscopic (SEM) pictures. An ORION Model 720A pH/ion meter and a combined glass electrode were used to obtain the pH readings. The pH-meter was calibrated with commercial pH 4.0; 7.0 and 10.0 buffer solutions prior to the measurements. When not in use, the glass electrode was immersed in deionized water.

2. 3. Graphene Oxide Synthesis

Graphene oxide is synthesized from graphite powder using a modified Hummer process.[47] 5 g graphite powder, 2.5 g sodium nitrate ($NaNO_3$), and 115 mL 96.4% sulfuric acid (H_2SO_4) were mixed in the first step of the synthesis process. In an ice bath, the entire mixture was agitated for

1 hour and, 15 g potassium permanganate ($KMnO_4$) was gently added to the mixture. The temperature was kept below 5 °C for the permanganate addition. The solution was taken out of the ice bath and stired for 2 hours until it turned dark green.

The temperature of the mixture was kept between 35–40 °C during these procedures. 500 mL deionized water was gently added to the mixture in the second step of the synthesis process, and stirring was continued for 1 hour. To remove excess $KMnO_4$, 8.4 mL of hydrogen peroxide (H_2O_2, 35.7%) was gently dropped and stirred for 10 minutes. The exothermic process happened, and the temperature was allowed to fall to room temperature.

Following a 10-minute centrifugation at 5000 rpm, 10 mL hydrochloric acid and 30 mL deionized water were added. After that, the supernatant was decanted, and the remaining residue was rewashed three times with an HCl/deionized water mixture until pH 7 was achieved. As a result, the prepared GO was vacuum-dried overnight at 50 °C for 24 hours.

2. 4. Characterization of Graphene Oxide

Graphene oxide nanostructures were investigated using a Zeiss Evo 60 EP model Scanning Electron Microscope (SEM) with magnifications of 2500 X and accelerating voltages of 15 kV.

2. 5. RGO/AuNPs/GCE Nanocomposite Sensor Fabrication

The non-modified GCE (nGCE) was polished manually with Al_2O_3 suspension (0.3 m, ATM GMBH, Germany), rinsed with deionized water, and sonicated in ethanol and double-distilled water for 5 minutes, respectively.

GO was dispersed into sodium acetate buffer by stirring at room temperature, and the resultant liquid was ultrasonicated for 4 hours, providing a homogeneous black dispersion containing 1 mg mL^{-1} GO.

The buffer solution of sodium acetate serves as both a buffer and an intercalant. The intercalation of sodium ions inhibits restacking of the electrochemically reduced graphene sheets, resulting in a larger electrochemically active surface area for the RGO modified electrode. The electrode was cleaned with deionized water after electrochemical reduction and placed in a 50°C oven for 15 minutes to thoroughly evaporate the solvent and increase RGO molecule adherence to the electrode surface.

The GO dispersion was then dropped 5 µL onto a pre-cleaned GCE and let to dry at room temperature. The GO/GCE was placed in an electrochemical cell containing an acetate buffer solution (pH = 5) and 50 cyclic voltammetric scans between (+0.4) V and (–0.4) V were done at a scan rate of 0.050 V/s. As a result, the GO treated GCE was electrochemically reduced to RGO and dried in the open air for 10 minutes. RGO/GCE was then immersed in a 3 mmol L^{-1} $HAuClO_4.H_2O$ solution prepared in 0.01 mol L^{-1} Na_2SO_4 and 0.01 mol L^{-1} H_2SO_4 solution in the measurement cell. To electrodeposit Au nanoparticles (AuNPs) on the RGO/GCE, 20 consecutive cycles in the potential range of 0.2 to +1.0 V at a scan rate of 0.050 V s^{-1} were utilized. The modified sensor was labeled RGO/GCE/AuNPs, dried, and used as an electrochemical sensor. When it wasn't in use, the sensor was kept at room temperature.

2. 6. Electrochemical Measurements

Appropriate volumes of supporting electrolyte (KCl) and pesticide standard solution were added to the electrochemical cell with a total volume of 5.0 mL in the cyclic voltammetry and differential pulse voltammetry methods used in this study. To record the background signals, voltammogram of the supporting electrolyte was obtained before adding the pesticide solution to be examined. At a scanning rate of 0.050 V s^{-1}, cyclic voltammetric measurements were taken. According to the potential signaled by the pesticides, the most appropriate potential range was employed in both methods. Cyclic voltammograms of the GCE and modified electrode were acquired by scanning the potential between 0.80 V and +1.00 V vs. Ag/AgCl at a scan rate of 0.050 V s^{-1}. All other voltammetric measurements were performed in a BR buffer solution at room temperature (25 ± 1 °C) (0.04 mol L^{-1}, pH 8.0)

2. 7. Optimization of the Experimental Conditions for Ziram

To create a highly sensitive method with a low detection limit, it's crucial to identify the most effective experimental conditions. On bare and modified GCE, the effect of scan rate, pH, and supporting electrolyte on the voltammetric response of ziram was examined. The sensitivity of the assay was shown by putting the constructed sensor to the test with real samples.

2. 8. Real Sample Application of the Sensor

Tap water and peach juice samples were analyzed using the spiking approach to determine the applicability of the RGO/AuNPs/GCE sensor.

Tap water samples were taken from our laboratory and spiked with a certain amount of standard ziram solution. To maintain a homogeneous mixture, it was agitated for 3 hours in an ultrasonic bath. This solution was added to electrochemical cells containing 100 mM KCl in Britton-Robinson (BR) buffer solution (0.04 mol L^{-1}, pH 8.0) in quantities of 250 µL, 500 µL, and 1500 µL. The DPV method was used to analyze the samples.

Peach juice was also tested to the method's application. Peaches were picked from a farmer's garden that practices organic farming and avoids using pesticides. The

peach juice obtained by squeezing the fruit was filtered through the filter paper and the pulp was removed. In 25 mL of peach juice, a known amount of 1.01 mM ziram stock solution was added. To get a homogenous mixture, it was sonicated for 2–3 hours in an ultrasonic bath. 25 mL acetone was added to the mixture before it was transferred to centrifuge tubes. The organic phase was filtered via a Buchner funnel using Whatman filter paper (No.4) after centrifugation at 4000 rpm for 10 minutes. To remove the solvent, the filtrate was transferred to a 250 mL rotating vacuum evaporator vessel. After the solvent had evaporated, the residue was dissolved in acetone to yield a total volume of 5.0 mL. The blank sample was made by following the identical steps as the peach juice sample that did not contain ziram.

3. Results and Discussion

3. 1. Characterization of Graphene Oxide

SEM image of the prepared GO is presented Figure 1. From the SEM image it is evident that GO has a multiple lamellar layer structure and it is possible to distinguish the edges of individual sheets. The layers are stacked one above the other and also show wrinkled areas, which could be attributed to intrinsic and extrinsic factors such as thermal fluctuation, defects, and functionalization. The wrinkled structure of the GO can increase the effective surface area and thus provide a good platform for bonding the AuNPs.

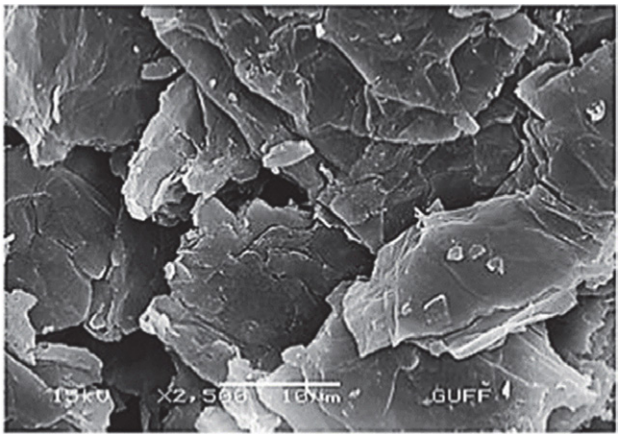

Figure 1. SEM images of synthesized graphene oxide.

3. 2. Optimization of RGO/AuNPs Sensor Fabrication

The electropolimerization cycles were investigated to achieve the best responses for ziram determination. Effect of GO concentration on sensor response was investigated using 0.5 mg mL^{-1}; 1.0 mg mL^{-1}; 1.5 mg mL^{-1}; and 2.0 mg mL^{-1}. The highest current response was observed with the electrode prepared with 1.0 mg mL^{-1} GO and this value was selected as the optimum GO concentration (Fig. 2). GO concentration higher than 1.0 mg mL^{-1} did not increase the sensor response. The results could be attributed to the thicker RGO layer, which restricted electrical conductivity.

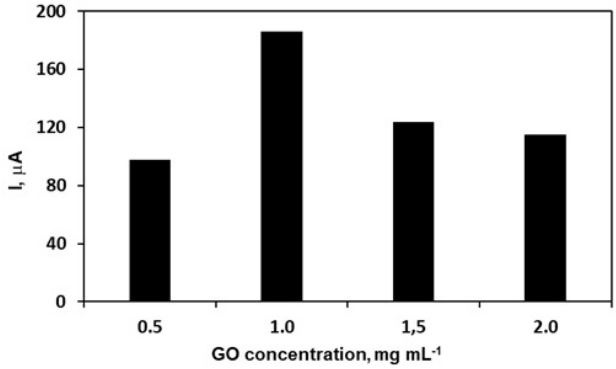

Figure 2. Effect of GO concentration on the response of the RGO/GCE.

Fig. 3 shows the cyclic voltammogram of electrochemical reduction peak of graphene oxide at –1.14 V. Electrons act as a reducing agent, causing RGO to occur on the GCE surface. Wang et al. reported the electrochemical reduction mechanism of graphene oxide with two assumptions.[48] The reduction of newly formed hydrogen atoms produced near the electrode surface during the water electrolysis process was one of the expectations. The following reaction takes place during water electrolysis.

$$2H_2O + 2e^- \rightarrow H_{2(g)} + 2OH^-$$

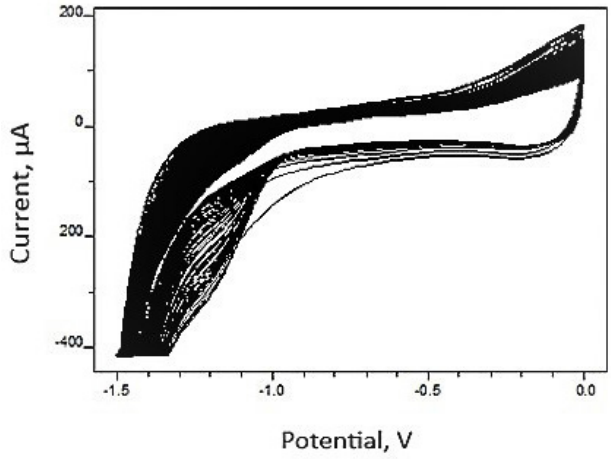

Figure 3. CV of electrochemical reduction of 1.0 mg mL^{-1} graphene oxide on GCE surface in acetate buffer solution (pH = 5) at the scan rate of 0.050 V s^{-1} in the potential range of (–1.2) – (2.2) V.

Hydrogen gas produced at the edges of graphene oxide can also contribute to the reduction process of graphene oxide.

During the electrochemical reduction process, a cathodic peak was observed due to the formation of reduced graphene oxide. The continuous deposition of conducting reduced graphene oxide on the electrode surface was evidenced by the linear increase in peak current with consecutive cycles. The current intensity stabilized after approximately 15–20 cycles and the electrochemically active surface area reached its maximum value. Then, the RGO/GCE was washed with ultrapure water. According to the literature, gold nanoparticles were successfully deposited on the RGO/GCE surface.[49]

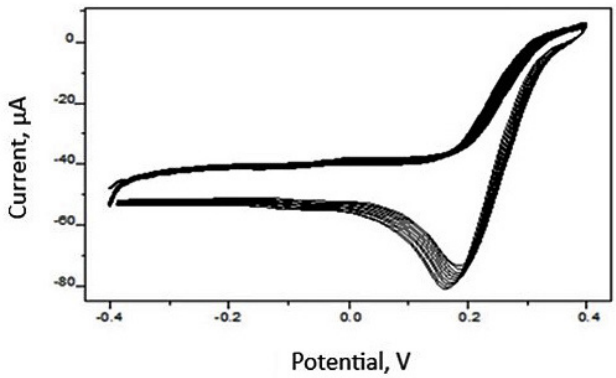

Figure 4. Repetitive cyclic voltammogram of RGO/GCE in 0.01 mol L^{-1} H_2SO_4 solution containing 3 mmol L^{-1} $HAuClO_4$ and 0.01 mol L^{-1} Na_2SO_4 at a scan rate of 0.050 V s^{-1} in the potential range of (–0.4) – (0.4) V.

3. 3. Electrochemical Characterization of RGO/AuNPs/GCE

Nanocomposite

The cyclic voltammogram (CV) of the $[Fe(CN)_6]^{3-/4-}$ redox probe is a useful method for investigating the characteristics of surface-modified electrodes. For this, electrochemical characteristics of the modified and unmodified sensors were investigated in 100 mM KCl containing 5.0 mM of $[Fe(CN)_6]^{3-/4-}$ ions. Figure 5 shows the CVs recorded for GCE, RGO/GCE, and AuNPs/RGO/GCE. In these three voltammograms, reversible peaks of $[Fe(CN)_6]^{3-/4-}$ were observed. Although all voltammograms showed a pair of redox peaks corresponding to Fe^{3+}/Fe^{2+}, the current intensity varied.

Because of the RGO's large surface area and great conductivity, it was observed that peak currents increased slightly once the GCE surface was modified with RGO. When the surface was modified with gold nanoparticles, the peak currents were significantly increased compared to the currents obtained with GCE and RGO/GCE. These changes can be interpreted as that AuNPs assisting electron transfer between the redox probe and the electrode. This finding supports the idea that combining the two nanomaterials, RGO and AuNPs, increased the electrode's sensitivity by raising the current intensity or enhance the current due to electro catalytical effect and large surface area.[50]

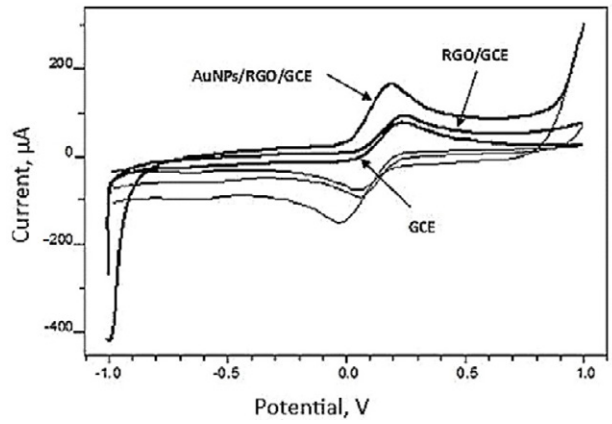

Figure 5. Cyclic voltammograms of GCE, RGO/GCE and AuNPs/RGO/GCE in 5.0 mM $[Fe(CN)_6]^{3-/4-}$ containing 100 mM KCl.

3. 4. Electrochemical Performance of the Sensors

In 0.04 mol L^{-1} BR buffer solution (pH 8.0), the CV responses of the bare GCE, RGO/GCE, and AuNPs/RGO/GCE sensors to 1.50×10^{-3} mol L^{-1} ziram were individually examined. Figure 6 depicts a comparison of voltammograms obtained using GCE, RGO/GCE, and AuNPs/RGO/GCE sensors under the same experimental conditions. The anodic peak current of ziram was investigated using the CV results. Because of the distribution of AuNPs on the electrode surface, the current measured at AuNPs modified RGO/GCE was significantly higher than the current measured at RGO/GCE and bare GCE. As a result of their distinctive properties, the simultaneous presence of RGO and AuNPs improved the sensitivity of ziram detection. A synergic effect of their combination was demonstrated as a result of a larger surface area and increased conductivity.

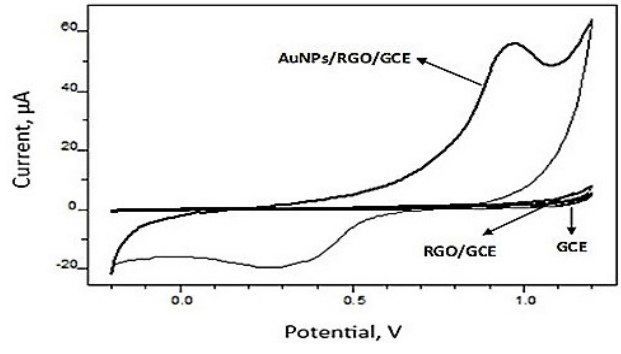

Figure 6. The cyclic voltammograms of 1.50×10^{-3} mol L^{-1} ziram in BR buffer solution with pH 8.0 at scan rate 0.050 v s^{-1}, for the bare GCE, RGO/GCE and AuNPs/RGO/GCE.

3. 5. Optimization of Experimental Conditions

The pH of the supporting solution has critical importance in obtaining good analytical performance for a developed sensor. Therefore, the effect of pH was investigated for ziram in 0.04 mol L^{-1} BR buffer solutions. This study was carried out at 1.52×10^{-3} mol L^{-1} constant ziram concentration over the pH range from 5.0 to 10.0. The variation of peak currents and peak potentials of the voltammograms recorded for the ziram oxidation were given in Table 1. The current response of the AuNPs/RGO/GCE sensor increased with the pH increasing from 5.0 to 8.0 and then gradually decreased from 8.0 to 10.0 (Fig. 7). As seen from the Figure, at pH 5.0 AuNPs/RGO/GCE sensor showed small anodic peak at around 0.72 V. But increase of pH value causes increase of peak currents up to pH 8.0. Only a fluctuation was observed for the peak potential at pH 7.0. The voltammetric response was pH sensitive and maximum peak current was appeared at pH 8.01. As a result, BR buffer solution at pH 8.01 was chosen for the following work. The ziram's oxidation peak potential shifted to less negative values ranging from 8.0 to 10.0, indicating proton transfer participation in the electrode reaction.

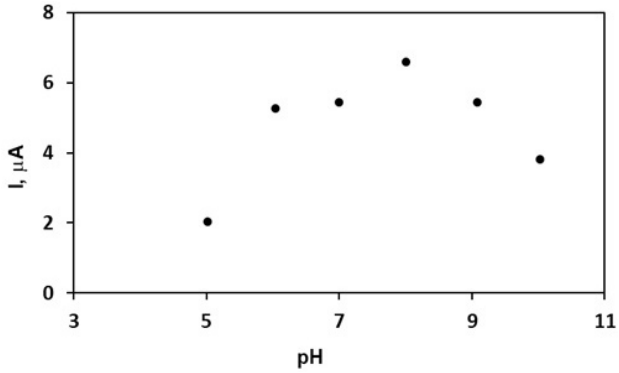

Figure 7. Effect of pH of ziram solutions on the current intensity of AuNPs/RGO/GCE

Table 1. Variation of peak potential and peak current of 1.52×10^{-3} mol L^{-1} ziram solution at a scan rate of 0.050 V s^{-1} and different pH in 0.04 mol L^{-1} BR buffer solutions.

pH	Peak current (µA)	Peak potential (V)
5.01	2.027	0.722
6.04	5.256	0.744
7.00	5.445	0.676
8.01	6.605	0.710
9.08	5.430	0.652
10.03	3.815	0.648

The scan rate is an important parameter to evaluate the electrochemical behaviour, adsorption and diffusion properties of ziram on the electrode surface. Therefore, the effect of scan rate on the oxidation peak current of 1.0×10^{-4} mol L^{-1} ziram was studied. The variation of the peak current of ziram versus the square root of the scan rate was plotted (Figure 8). It has been observed that with the scan rate increasing, the anodic peak current increased. In the 0.050–0.300 V s^{-1} range, there was good linearity between the square root of scan rate and peak current. The linear regression equation was (µA) = 0.2783 (µA s) 0.0785 (µA) with correlation coefficient 0.9919. The correlation coefficient is very close to 1.0, indicating that the oxidation process is controlled by diffusion.[51,52]

In addition, it was observed that logarithm of peak current changed linearly with the logarithm of scan rate and slope value for this linear line is 0.6346. For ideal diffusion-controlled the slope is between 0.5 and 1.0.[53]

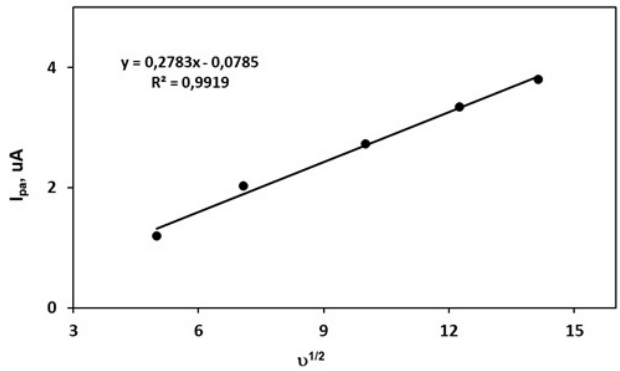

Figure 8. Variation of anodic peak current (I_{pa})*versus* the square root of scan rate ($\upsilon^{1/2}$)

3. 6. Analytical Performance Parameters of the Sensor

The correlation between ziram concentrations and anodic peak currents was examined utilizing the DPV method in BR buffer solution (pH 8.0) with the AuNPs/RGO/GCE composite sensor under optimized experimental conditions. The calibration graph was shown in Fig. 9. Over the range of 1.50×10^{-5} mol L^{-1} to 1.63×10^{-7} mol L^{-1}, the peak current increases linearly with the increasing ziram concentration. The linearity between the anodic peak current and the ziram concentration is shown in the following equation;

$$I_{pa}(\mu A) = 2x10^{7}.C_{ziram}(\mu M) + 5.5336 \quad (R^2 = 0.9996) \qquad (1)$$

The linear range of the calibration curve is 1.50×10^{-5} mol L^{-1} to 1.63×10^{-7} mol L^{-1} with the LOD values of 1.19×10^{-7} mol L^{-1} for ziram. The formulas (3 × s/m) and (10 × s/m) were used to calculate the method's limit of detection (LOD) and limit of quantification (LOQ).[54] Where ***s*** denotes the measurement's standard deviation and ***m*** denotes the calibration curve's slope (or the sensitivity).

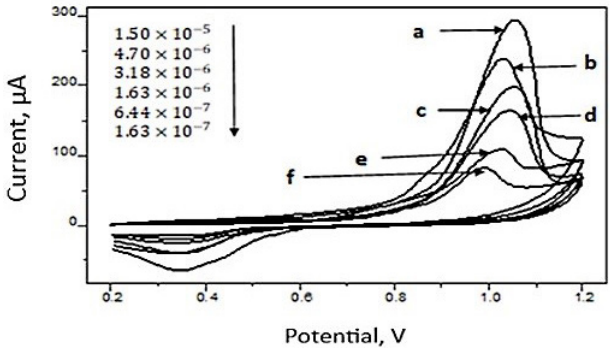

Figure 9. The calibration voltammograms at different concentrations of ziram in BR buffer (pH 8) at AuNPs/RGO/GCE by DPV (a)1.50×10^{-5}; (b) 4.70×10^{-6}; (c) 3.18×10^{-6}; (d) 1.63×10^{-6}; (e) 6.44×10^{-7}; (f)1.63×10^{-7} mol L^{-1}.

LOD value satisfies the MRLs established by the The Codex Alimentarius Commision (CAC), for stone fruits (7.0 mg kg^{-1}).[55] Particular pesticide limit levels have also been set at 0.1 µg L^{-1} by the European Union. This value was decided as the LOD for all pesticides found in drinking water. That means the method is sensitive enough and the developed sensor can be used with high reliability in detecting the maximum allowable residue level of ziram in fresh fruits and water. All validation and regression parameters are tabulated in Table 2.

Table 2. Analytical performance of the RGO/AuNPs/GCE sensor for ziram.

Parameters	Value
Linear working range, mol L^{-1}	$1.50 \times 10^{-5} - 1.63 \times 10^{-7}$
LOD (mol L^{-1})	1.19×10^{-7}
LOQ (mol L^{-1})	7.80×10^{-7}
Calibration equation	I_{pa} (µA)= 2×10^{7} c_{ziram} (µM) + 5.5336
Regression coefficient (R^2)	0.9996
Selectivity (µA/µM)	2×10^{7}
Intercept	5.5336
Reproducibility (RSD, %)	2.35
Repeatability (RSD, %)	4.12

3. 7. Reproducibility and Repeatability

To demonstrate the reproducibility of the RGO/AuNPs/GCE sensor, 3 modified electrodes were prepared under the same composition. Under optimized experimental conditions, repeated DPV measurements (n = 5) from a solution that contains 5.0×10^{-4} mol L^{-1} ziram were used to identify the peak current for each electrode. The anodic peak currents for ziram had a relative standard deviation (RSD) of 2.35% (Table 2). This implies that the electrode has a high level of repeatability. Multiple DPV measurements (n = 5) were used to assess the sensor's repeatability, giving RSD value of 4.12% (Table 2).

3. 8. Real Sample Analysis

The analytical applicability of the prepared sensor was performed with tap water and peach juice. The recovery of the method was evaluated by spiking tap water and peach juice samples with ziram at low, middle and high concentration levels of the calibration graph. Calculated recovery values and added ziram concentrations are given in Table 3 and Table 4.

The obtained recovery values were between 96.4 and 107.6%. These results show that the developed electrochemical sensor can effectively be applied with high sensitivity and selectivity for ziram determination in two different matrices.

Table 3. Recovery results obtained by standard addition method in tap water sample using RGO/AuNPs/GCE sensor.

No	Added ziram, (mg L^{-1})	Found ziram, (mg L^{-1})	Recovery, %	RSD, %	Relative error, %
1	0.56	0.54 (±0.02)	96.4 (±2.73)	2.83	–3.6
2	1.68	1.64 (±0.02)	97.6 (±1.19)	1.22	–2.4
3	2.50	2.69 (±0.04)	107.6 (±1.67)	1.55	7.6

* The average of three measurements is used for each value.
RSD, Relative Standard Deviation

Table 4. Recovery values obtained by standard addition method in peach juice using RGO/AuNPs/GCE sensor.

No	Added ziram, (mg L^{-1})	Found ziram, (mg L^{-1})	Recovery, %	RSD, %	Relative error, %
1	0.62	0.65 (±0.03)	104.8 (±4.3)	4.07	4.84
2	1.86	1.83 (±0.03)	98.8 (±1.6)	1.64	–1.61
3	2.48	2.37 (±0.04)	95.3 (±1.6)	1.71	–4.70

* The average of three measurements is used for each value.
RSD, Relative Standard Deviation

4. Conclusion

A sensitive electrochemical sensor for the rapid detection of ziram was successfully constructed by modifying AuNPs improved RGO on GCE. Using cyclic voltammetry and differential pulse voltammetry, the electrochemical behaviour and real sample applicability of RGO/AuNPs/GCE were examined. The proposed electrochemical method was validated and the constructed sensor was proven to have good sensitivity and selectivity, as well as a low detection limit. Furthermore, the method has been used

to accurately determine the ziram in spiked tap water and peach juice. The created RGO/AuNPs/GCE sensor is effective and promising due to its relatively simple modification method and disposable feature, as well as its potential to be used for direct measurements in water and peach juice. The findings of this study add to the analytical methodologies for ziram determination that have been used thus far.

Data available on request from the authors

The data that support the findings of this study are available from the corresponding author, [Aslan, N.], upon reasonable request.

Nazife Aslan http://orcid.org/0000-0002-2622-5908

Declaration of competing interest

The authors declare that they have no known competing financial interests or personal relationships that could have appeared to influence the work reported in this article.

The authors also declare that they have no conflict of interest with suggested reviewers.

Acknowledgements

The authors express their gratitude for the support from Gazi University with Grand Numbers BAP- 65/2020-03.

5. References

1. T. A. Saleh, V. K. Gupta, *Nanomaterial and Polymer Membranes* **2016,** 83–133; **DOI:**10.1016/B978-0-12-804703-3.00004-8
2. M. H. Mahnashi, A. M. Mahmoud, A. Az, K. Alhazzani, S. A. Alanazi, M. M. Alanazi, M. M. El-Wekil, *Microchemical Journal* **2021,** *164,* 106020–106025; **DOI:**10.1016/j.microc.2021.106020
3. O. Arjmand, M. Ardjmand, A. M. Amani, M. H. Eikani, *Acta Chim. Slov.* **2020**, *67,* 496–506; **DOI:**10.17344/acsi.2019.5513
4. V. Vukojevića, S. Djurdjića, M. Ognjanović, M. Fabiánb, A. Samphaod, K. Kalchere, D. M. Stanković, *Journal of Electroanalytical Chemistry* **2018,** *823*, 610–616; **DOI:**10.1016/j.jelechem.2018.07.013
5. P. K. Kalambate, B. J. Sanghavi, S. P. Karna, A. K. Srivastava, *Sens. Actuators B* **2015,** *213*, 285–294; **DOI:**10.1016/j.snb.2015.02.090
6. X. Ye, Y. Du, D. Lu, C. Wang, *Anal. Chim. Acta* **2013,** *779*, 22–34; **DOI:**10.1016/j.aca.2013.03.061
7. R. Sengupta, M. Bhattacharya, S. Bandyopadhyay, A. K. Bhowmick, *Prog. Polym. Sci.* **2011,** *36(5)*, 638–670; **DOI:**10.1016/j.progpolymsci.2010.11.003
8. P. J. Wessely, U. Schwalke, *Appl. Surf. Sci.* **2014**, *291*, 83–86; **DOI:**10.1016/j.apsusc.2013.09.142
9. S. F. Pei, H. M. Cheng, *Carbon* **2012**, *50(9)*, 3210–3228; **DOI:**10.1016/j.carbon.2011.11.010
10. S. L. Yang, S. L. Luo, C. B. Liu, W. Z. Wei, *Colloid Surface B* **2012**, *96*, 75–79; **DOI:**10.1016/j.colsurfb.2012.03.007
11. V. Stanković, S. Đurđić, M. Ognjanović, J. Mutić, K. Kalcher, D. M. Stanković, *Journal of Electroanalytical Chemistry* **2020,** *876*, 114487–114493; **DOI:**10.1016/j.jelechem.2020.114487
12. A. M. Mahmoud, M. M. El-Wekil, M. H. Mahnashi, M. F. B. Ali, S. A. Alkahtani, *Microchimica Acta* **2019**, *186*, 617–624. **DOI:**10.1007/s00604-019-3647-7
13. Y. Liu, G. Gao, J. Hu and X. Z, *Int. J. Electrochem. Sci.* **2018,** *13*, 11853–11866; **DOI:**10.20964/2018.12.05
14. Y. Zhou, M. Ma, H. He, Z. Cai, N. Gao, C. He, G. Chang, X. Wang, Y. He*, Biosensors and Bioelectronics* **2019***, 146,* 111751; **DOI:**10.1016/j.bios.2019.111751
15. R. Wang, Z. Wu, C. Chen, Z. Qin, H. Zhu, Guo. Wang, C. Wu, W. Dong, W. Fan and J. Wang, *Chem. Commun*. **2013** *49*, 8250–8252; **DOI:**10.20964/2018.12.05
16. Y. Liu, G, Gao, J. Hu, X. Zou, *Int. J. Electrochem. Sci.,* **2018,** *13,* 11853 – 11866; **DOI:**10.20964/2018.12.05
17. E. Er, H. Çelikkan, N. Erk, M. Levent Aksu, *Electrochim Acta* **2015,** *157*, 252–257; **DOI:**10.1016/j.electacta.2015.01.020
18. P. Sharma, G. Darabdhara, T.M. Reddt, A. Borah, P. Bezboruah, P. Gogoi, N. Hussain, P. Sengupta, M.R. Das, *Catal. Commun.* **2013,** *40*, 139–144; **DOI:**10.1016/j.catcom.2013.06.021
19. P. Dong, B. Jiang, J. Zheng, Anal. Methods, **2019,** *11*, 2428–2434; **DOI:**10.1039/C9AY00549H
20. B. Jiang, P. Dong, J. Zheng, Talanta **2018,** *183,* 114–121; **DOI:**10.1016/j.talanta.2018.02.016
21. J. Lu, Y. Sun, G.I.N. Waterhouse, Z. Xu, Adv. Polym. Technol. **2018**, *37*, 3629–3638; **DOI:**10.1002/adv.22147
22. M-S. Tsaia, C-J. Lua, P-G. Sub, *Materials Chemistry and Physics* **2018***, 215,* 293–298; **DOI:**10.1016/j.matchemphys.2018.05.058
23. Y. Gao, X. Wu, H. Wang, W. Lu and M. Guo, *Analyst* **2018**, *143*, 297–303; **DOI:**10.1039/C7AN01706E
24. M.H. Ghanbaria, A. Khoshrooc, H. Sobatid, M.R. Ganjalie, M. Rahimi-Nasrabadi, F. Ahmadi, *Microchemical Journal* **2019**, 147, 198–206; **DOI:**10.1016/j.microc.2019.03.016
25. F. Gendi, D-W. Sun, H. Pu, Q. Wei, *Talanta* **2019,** *195(1),* 841–849; **DOI:**10.1016/j.talanta.2018.11.114
26. A. Hussain, H. Pu, D-W. Sun, *Food Chemistry* **2020,** *317,* 126429; **DOI:**10.1016/j.foodchem.2020.126429
27. P. Fanjul-Bolado, R. Fogel, J. Limson, C. Purcarea, A. Vasilescu, *Biosensors* **2021,** *11(1)*, 12–37. **DOI:**10.3390/bios11010012
28. C. A. Martin, K. M. Myers, A. Chen, N. T. Martin, A. Barajas, D. E. Krantz, *Experimental Neurology* **2016,** *275(1)*, 232–241; **DOI:**10.1016/j.expneurol.2015.09.017
29. A. Scheyer, C. Graeff, S. Morv, *Chemosphere* **2005,** *58*, 1517–1524; **DOI:**10.1016/j.chemosphere.2004.10.013
30. K. Wang, D-W. Sun, H. Pu, Q. Wei, *Food Chem.* **2020**, *310*, 125923; **DOI:**10.1016/j.foodchem.2019.125923
31. USEPA, Code of Federal Regulations: Part 180-Tolerances and Exemptions for Pesticide Chemical Residues in Food **2014**, *24* (Available at https://www.ecfr.gov/cgi-bin/text-idx?)

32. C. A. Martin, K. M. Myers, A. Chen, N. T. Martin, A. Barajas, D. E. Krantz, *Exp. Neurol.* **2016**, *275*, 232–241; **DOI:**10.1016/j.expneurol.2015.09.017
33. J. Al-Alam, L. Bom, A. Chbani, Z. Fajloun, M. Millet, *J. Chromatogr. Sci.* **2017,** *55(4)*, 429–435; **DOI:**10.3390/polym11091449
34. B. Schmidt, H. B. Christensen, A. Petersen, J. J. Sloth, M. E. *Food Additives & Contaminants: Part A* **2013**, *30(7)*; 1287–1298. **DOI:**10.1080/19440049.2013.801083
35. Y. Nolvachai, C. Kulsing, P. J. Marriott, *Crit. Rev. Environ. Sci. Technol.* **2015**, *45(19)*, 2135–2173; **DOI:**10.1080/10643389.2015.1010431
36. J. Chen, F. Fu, S. Wu, J. Wang, Z. Wang, *J. Sep. Sci.* **2017,** *40(19)*, 3898–3904; **DOI:**10.1002/jssc.201700455
37. L. M. Silva, D. De Souza, *Electrochimica Acta* **2017**, *224,* 541–550; **DOI:**10.1016/j.electacta.2016.11.133
38. D. Amorello, S. Orecchio, *Microchemical Journal* **2013,** *110*, 334–339; **DOI:**10.1016/j.microc.2013.05.002
39. P. Qiu, Y. N. Ni, *Chin. Chem. Lett.* **2008,** *19(11)*, 1337–1340; **DOI:**10.1016/j.cclet.2008.07.013
40. D. M. Stankovi´c, K. Kalcher, *Sens. Actuators B* **2016,** *233*, 144–147; **DOI:**10.1016/j.snb.2016.04.069
41. L. Janíková-Bandžuchová, R. Šelešovská, K. Schwarzová-Pecková, J. Chýlková, *Electrochimica Acta* **2015,** *154*, 421–429; **DOI:**10.1016/j.electacta.2014.12.064
42. A. Vasilescu, A. M. Titoiu, C. Purcarea, G. Necula-Petrareanu, Romanian OSIM Patent Application No. A/00587, 13 August **2018**
43. R. Šelešovská, K. Schwarzová-Pecková, R. Sokolová, K. Krejčová, P. Martinková-Kelíšková, *Electrochimica Acta* **2015,** *381(10)*, 138260; **DOI:**10.1016/j.electacta.2021.138260
44. N. S. Khan, D. Pradhan, S. Choudhary, P. Saxena, N. K. Poddar, A. K. Jain, *Journal of Analytical Science and Technology* **2021**, 12–32. **DOI:**10.1186/s40543-021-00282-6
45. L. G. Shaidarova, G. K. Budnikov, S. A. Zaripova, *J. Anal.Chem.* **2001,** *56(8)*; 748–753. **DOI:**10.1023/A:1016741828696
46. S. Wyantuti, R.Tjokronegoro, S. Rochani, *Proceeding of The International Seminar on Chemistry* **2008**, 374–376.
47. N. I. Zaabaa, K. L. Fooa, U. Hashimad, S. J. Tanbc, W. W. Liu, C. H. Voona, *Solvent Influence* **2017**, *8*, 469–477; **DOI:**10.1016/j.proeng.2017.04.118
48. Y. Xu, H. Bai, G. Lu, C. Li, G. Shi, *J. Am. Chem. Soc.* **2008,** *130(18)*; 5856–5857. **DOI:**10.1021/ja800745y
49. X. Wang, I. Kholmanov, H. Chou, S. R. Rodney, *ACS Nano* **2015,** *9(9)*; 87378743; **DOI:**10.1021/acsnano.5b03814
50. J. Wang, *Analytical Electrochemistry*, Wiley-VCH, New York 2000
51. I. H. Taşdemir, M. A. Akay, N. Erk, E. Kılıç, *Electroanalysis* **2010**, *22(17–18)*; 2101–2109. **DOI:**10.1002/elan.201000100
52. Y. Jiang, D. Shengyuan, L. Janping, J. Huangxian, G. Sundaram, *Biosens. Bioelectron.* **2011**, *29(1)*, 159–166; **DOI:**10.1016/j.bios.2011.08.011
53. D. Caschera, F. Federici, D. Zane, F. Focanti, A. Curulli, G. Padeletti, *J. Nanopart. Res.* **2009,** 11, 1925–1936; **DOI:**10.1007/s11051-008-9547-0
54. M. H. Mahnashi, A.M. Mahmoud, S.A. Alkahtani, R. Ali, M. M. El-Wekil, *Anal. Bioanal. Chem.* **2020**, *412*, 355–364; **DOI:**10.1007/s00216-019-02245-8
55. Food and Agriculture Organization of the United Nations (FAO). www.fao.org/fao-who-codexalimentarius/codex-texts/dbs/pestres/pesticide-detail. (accessed December 22, **2021**).

Povzetek

V tem prispevku je opisana priprava senzorskih materialov na osnovi reduciranega grafenovega oksida z nanodelci zlata za določanje cinkovega(II)dimetilditiokarbamata (zirama). Grafenov oksid (GO) je bil sintetiziran po modificirani Hummerjevi metodi. Kompozitni senzor, sestavljen iz nanodelcev zlata (AuNP) in reduciranega grafenovega oksida (RGO), je bil elektrokemično izdelan na elektrodi iz steklenega ogljika. Nanokompozit je bil ovrednoten z uporabo vrstične elektronske mikroskopije (SEM). Ciklična voltametrija je bila uporabljena za prikaz elektrokemičnih lastnosti modificiranega senzorja na vsaki stopnji modifikacije. Predlagani senzor je pokazal dobro analitično zmogljivost za določanje pesticida ziram v vodi in breskovem soku, vključno z zelo nizko mejo zaznave, velikim linearnim razponom in nizkim RSD.